# Development of target fabrication for laser-driven inertial confinement fusion at research center of laser fusion

Tao Wang, Kai Du , Zhibing He, and Xiaoshan He

*Research Center of Laser Fusion, China Academy of Engineering Physics, Mianyang 621900, China*
*(Received 23 October 2016; revised 11 December 2016; accepted 17 January 2017)*

**Abstract**

As the basic conditions for laser inertial confinement fusion (ICF) research, the targets are required to be well specified and elaborately fabricated. Because of the characteristics of the targets, the research and fabrication process is a systematically tough task, which needs fundamental and deep insights into film deposition, mechanical machining, precise measurement and assembly, etc. As a result, knowledge of material science, physics, mechanical as well as electronics is a necessity for target researchers. In this paper, we give introductions to the state of art on target fabrication for ICF research at Research Center of Laser Fusion (RCLF) in China.

**Keywords:** development; ICF; target fabrication

## 1. Introduction

Controlled reaction of nuclear fusion is quite attractive in supply of abundant energy, which is also desirable in terms of safety and economic cost. The realization of such project could be helpful for our human being to deal with the ever worsening crisis of energy shortage and environmental pollution. At present, countries around the world have dedicated a lot into this campaign[1, 2].

The principle of inertial confinement fusion (ICF) is that a target shell filled with deuterium and tritium (DT) fuel is radioactively ablated by energetic laser beams with total energy of more than 1 MJ, plasma with ultra-high temperature and pressure is generated then, recoil force from this plasma could push the remaining capsule shell toward the center and compress the fuel to an extreme critical density, then hot spots with ultra-high temperature at parts of the fuel emerge and ignite all the fuel to nuclear fusion reaction, eventually nuclear energy is released to be utilized[2, 3]. There are two possible approaches for ignition by laser beams, i.e., direct drive and indirect drive. The first one is to ablate the target shell directly by laser beams, the other is to guide laser beams into a so-called hohlraum. The inner surface of the hohlraum translates the visible laser beams to energetic X-rays which then form a homogeneous radioactive field

inside the hohlraum; subsequently the target at the hohlraum center is ablated by the field to ignite the DT fuel[2].

Obviously, for either drive mode, target components are necessities. Development of targets with various critical features is determinable tasks for the implementation of the ignition. For the ultimate ignition, target capsules with diameter of ∼2 mm are required[4]. Before the banquet, multitudes of validating experiments must be performed, during which target capsules with diameter ranging from ∼300 µm to ∼2 mm, target components with varied dimensions and shapes such as cone, cylinder and plane are also on the request list. Due to the extreme conditions needed for the ignition, properties like material purity, surface quality, doping level and size of the target components required for the ICF experiments are inevitably specified rigorously[5, 6]. As a result, target fabrication is doomed to be tough mission involving several disciplines and engineering, which require unremitting efforts to fulfill.

Regarding the capability of target fabrication, the United States keeps ahead of any other countries. China has started researches on target production by the end of 1970s, and has made remarkable progresses since 1990s[7, 8]. Research Center of Laser Fusion (RCLF) is the exclusive institute dedicating to target design and fabrication in China. To date, we have built up versatile target fabrication facilities which enable us to be competent on producing target components with diverse patterns and compositions. These target components have persistently met rigid requirements from massive

Correspondence to: K. Du, Research Center of Laser Fusion, China Academy of Engineering Physics, Mianyang 621900, China.
Email: icf802@163.com

1

experiments carried out on several giant ICF laser facilities like SG-II and SG-III. In this paper, we give a systematic overview of recent development and difficulties on target fabrication at RCLF in China. The introduction will be mainly focused on topics as follows.

## 2. Fabrication of target shells

As mentioned above, target shells are designed as fuel containers for ICF experiments. Shells with diameter in scales of micrometer to millimeter are shot on different ICF facilities according to the energy output of the laser beams. Based on theoretical design, beryllium shell, glow discharge polymer (GDP) shell, glass shell, polystyrene (PS) and high density carbon (HDC) shell are chosen to be the candidates for the ultimate ignition. In the following, we introduce development of the last four shells.

*GDP shell*

Usually, inductive coupled plasma enhanced chemical vapor deposition (ICP-CVD) method is employed to fabricate GDP shells. As shown in Figure 1(a), the experimental setup is mainly composed of an RF power generator with tripled frequency (40.68 MHz), matching box, quartz tube circled with solenoid and reactive chamber. Trans-2-butene ($T_2B$) and $H_2$ are utilized as the working gases, the GDP coating is deposited on mandrels made from poly $\alpha$-methylstyrene (PAMS). It is worth noting that for early deposition of GDP coating, a cylindrical quartz tube with uniform diameter along its longitudinal direction is chosen as the plasma generator. At that time, growth rate of the coating was as slow as $\sim0.3$ m h$^{-1}$. Based on effortful simulations and explorations, the quartz tube was optimized to be cone-shaped which led to a dramatically fast growth rate of $\sim1.5$ m h$^{-1}$ and improved integral coating properties. In order to deposit coating on the mandrels homogeneously, the mandrels are agitated by a vacuum step motor to roll randomly inside a special designed glass pan as depicted in Figure 1(b). To acquire single layered GDP shells after the coating deposition, double layered PAMS/GDP capsules are annealed in vacuum or Ar atmosphere at 300 °C for more than 24 h to pyrolyze the mandrel.

For GDP shells requested by ICF experiments, properties like the surface roughness, microstructure, doping content, thermal and mechanical performance are the most concerned features. After years of investigations, effects of various key factors on these properties have been verified by us, and performance of the GDP shell has been improved step by step.

At the early stage, impacts of deposition parameters like the working pressure, flow ratio of the working gases as well as RF power on properties mentioned above of GDP

shells were thoroughly investigated. It was confirmed that as RF power increases, or working pressure decreases, or flow ratio of $T_2B$ decreases, content of polyethylene group inside the coating could be notably enhanced which leads to improved thermal and mechanical performance[9–12]. In fiscal year (FY) 2013, via further optimization of the mechanical property, fracture problem frequently occurred on thin-walled GDP shells during pyrolysis of PAMS mandrel was tackled. Consequently, only 8 µm thick single layered GDP shells with diameter of 450–540 µm were acquired.

Since the shells roll inside the pan continuously during the coating deposition, frictions among the shells and collisions from the pan surface have been confirmed to be the main causations for the nodular-like defects shown in Figure 2. Taking this conclusion into consideration, Zhang *et al.*[13, 14] has remarkably decreased the surface roughness of the GDP shells from $\sim200$ nm to smaller than 20 nm via intermittently agitating the shells by a modified inclined agitation setup.

Regarding the doping of the GDP shells, Zhang *et al.*[15, 16] have investigated the influences of working pressure, RF power, and flow ratio of the doping source on the coating properties. Further assisted by a precise mass flow controller with small full regulation range, they have successfully elaborated the quantitative relations between the process parameters and the doping amount. Eventually, GDP shells with a wide range of doping level (0.1–4.4 at. % of Si or 0.13–4.34 at. % of Ge) and graded doped GDP shells were fabricated. As displayed in Figure 3, GDP shell graded doped with Ge was characterized by cross-sectional scanning electron microscopy (SEM) and energy dispersive X-ray spectroscopy (EDS) scan.

*Hollow glass micro-sphere (HGM)*

Compared to other capsules, HGM has its own advantages like excellent symmetry, sound surface quality, large strength and mediate permeation to hydrogen isotope; thus it attracts nonstop research interests from target researchers.

HGM is used to be fabricated by drop tower technique which can be further sorted into liquid droplet method and dried gel method. These two sub methods have their own merits and drawbacks. Liquid droplet is superior in diameter and wall thickness control of the capsule; it is facile to produce capsules with uniform properties through this method, while dried gel has its advantage in content regulation of the glass shell. In fact, we have systematically explored both approaches at an early stage. For the research of liquid droplet, Qiu *et al.*[17, 18] have investigated the effects of solutions, tower structure, temperature distribution along the axial, gas content, distribution of the gas flow rate, vesicant type and amount, etc. on properties of the HGM. Based on their investigations, they have established an applicable process for HGM production. Regarding the dried gel method, Qi *et al.*[19, 20] have analyzed the thermal and
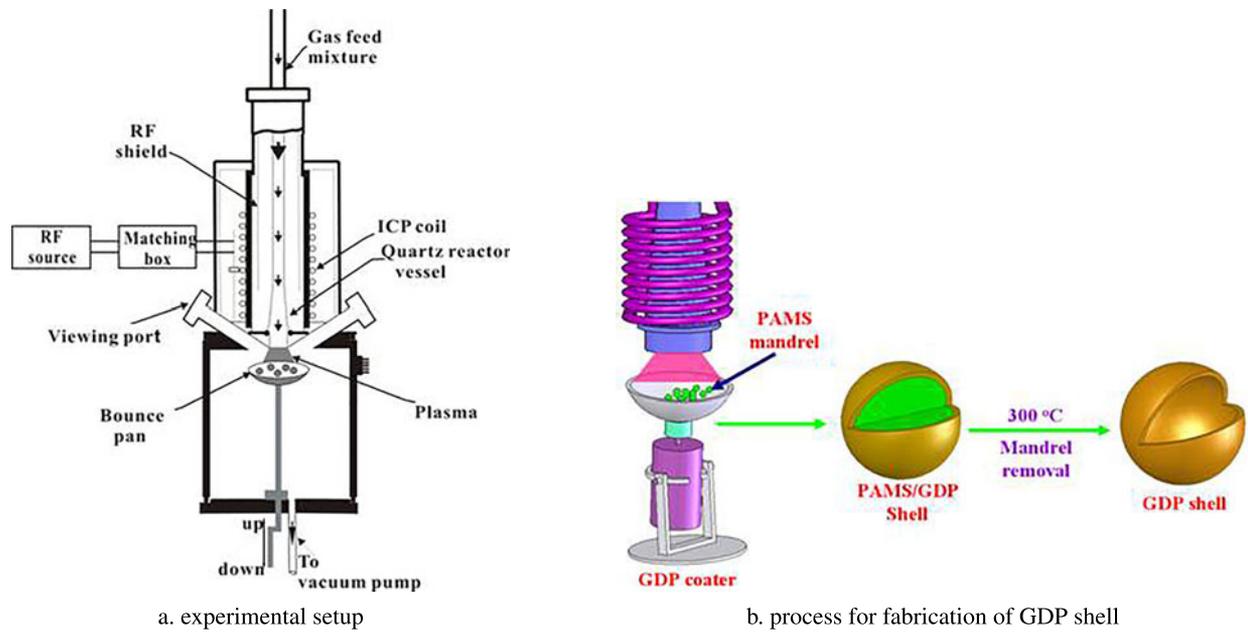
a. experimental setup

b. process for fabrication of GDP shell

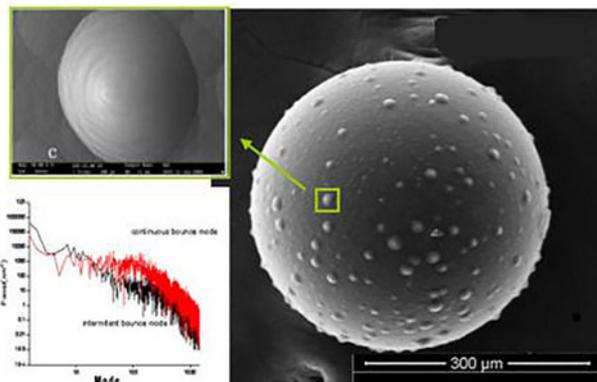**Figure 1.** Experimental setup and schematic process for fabrication of GDP shell.



**Figure 2.** Analysis of nodular-like defects on GDP surface by SEM scan and power spectrum.
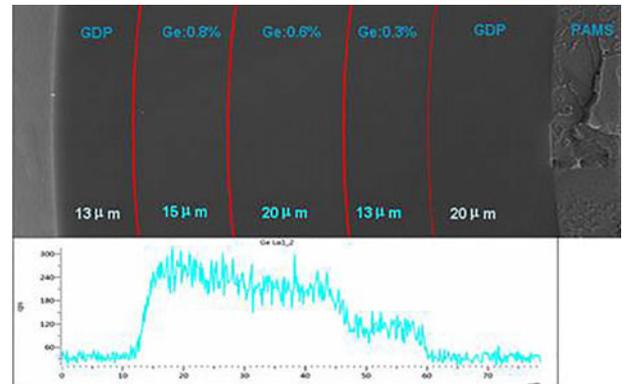


**Figure 3.** Cross-sectional SEM image and EDS results of GPD shell graded doped with Ge.

mass transmission, as well as movement and shape evolution of the gel particles during the processes of heat absorption, encapsulation, foaming, refining and cooling. As a result, they have built up a theoretical model for the capsule forming process inside the tower. They also have further discussed impacts of parameters like initial compositions and size of the gel particles, vesicant type and temperature, composition and pressure of the carrier gas, temperature and length of the high temperature region on the diameter and wall thickness of the HGM[21–24]. At present, both liquid droplet and dried gel methods are employed by us to fabricate HGM required by ICF experiments.

Since raw materials used in the liquid droplet method are required to be water soluble, it is difficult to adjust the contents and properties of the HGM. Moreover, it is

impossible to fabricate HGM with diameter larger than 500 $\mu$m, and thickness over 5 $\mu$m. For the dried gel method, the compositional inhomogeneity within the bulk gel always tends to cause performance variations among individual HGM and batches. Like liquid droplet, it is not easy to fabricate large size HGM with adjustable thickness for dried gel method either. Since FY2014, we have commenced to explore a new approach to make HGM, which was firstly reported by National Ignition Campaign (NIC) in the USA[25]. As illustrated in Figure 4, there are two decisive steps within the process. Firstly, Si:GDP coating with necessary thickness and Si content must be deposited on PAMS mandrels by CVD method interpreted above. Afterward, the prepared PAMS/ Si:GDP shell is sintered in a programmable oven under ramping temperatures to as
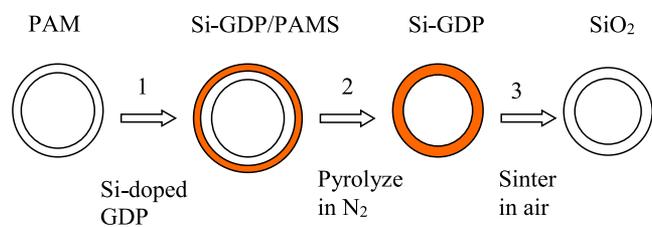
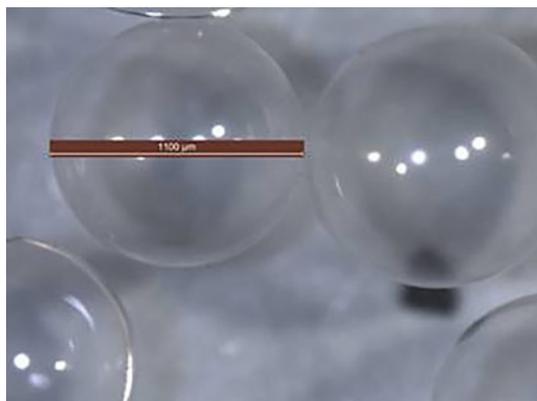**Figure 4.** Process for fabrication of HGM by Si:GDP method.



**Figure 5.** Photograph of HGM made by Si:GDP method.



**Figure 6.** XRF spectrum of an argon filled Si:GDP.

high as 1000 °C degrees centigrade with optimized ramping rate and holding time at certain temperatures. After this procedure, the PAMS mandrel is pyrolyzed away, and the Si:GDP shell is oxidized to a glass shell[26, 27]. As reported, it is promising to produce HGM with diameter ranging from hundreds of micrometers to several millimeters. Moreover, this method is also capable of making HGM with varied wall thickness. At RCLF, Xu *et al.*[28, 29] have investigated impacts of TMS flow rate and working pressure adopted during the process of Si:GDP deposition, and the sintering program on the shrinkage behavior of shell thickness & diameter, sphericity, composition, surface roughness and gas retention. Eventually, the integral process to produce HGM through this new technique has been mastered by us. At present, as presented in Figure 5, we are capable of fabricating HGM with thickness ranging from ∼5 to ∼20 μm, and diameter ranging from ∼500 μm to ∼1.5 mm. As confirmed by X-ray fluorescence (XRF) analysis displayed in Figure 6, Ar gas which is utilized as a diagnostic element in some experiments has also been filled inside the glass shell simultaneously along the sintering process.

*PS shell*

Generally, PS shells are fabricated by the micro-encapsulation technique, which includes an inner water phase (W1), an oil phase (O) and an outer water phase (W2). In fact, we have realized batch production of PS shells with this technique early.
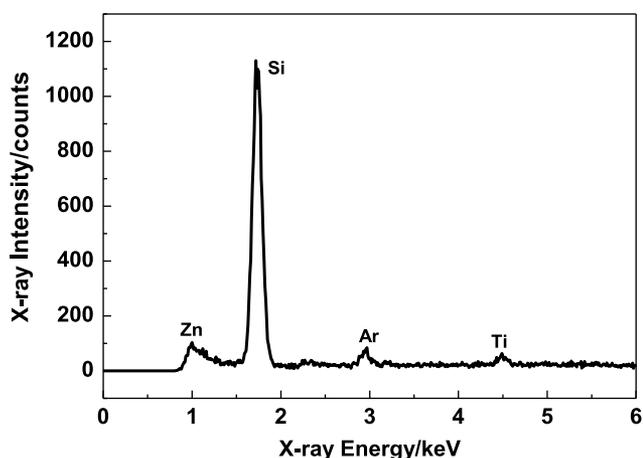
For some experiments, PS shells with different dopants are needed. In 2004, Li *et al.* performed an initial study on fabrication of inner Si-doped PS capsules[30]. Dimethyldiethoxysilane (DMDES) was utilized as the silicon donor in the study. After the shell fabrication, noncontact X-radiography and X-spectrum were employed to analyze the doping level. The results confirmed that Si content at the inner surface of the shell was 2–3 order higher than that at the outer surface, and thickness of the Si-doped layer was smaller than 0.3 μm. In 2009, using polystyrene sulfurnate (PSS) as the doping source, inner-S-doped PS capsules with a diameter of 200–800 μm were fabricated by Liu *et al.*[31]. They suggested that the doping uniformity can be affected by gravity, interfacial tension as well as the PSS concentration, and PS shell with uniform doping content at the inner surface can be obtained when the PSS concentration is 0.2%. Later in 2012, Chen *et al.* have further confirmed that the PSS concentration plays a key role in the S doping uniformity and the performance of the doped shell. Specifically, large PSS concentration always leads to brittle shells after thermal treatment[32].

As a matter of fact, fabrication of large diameter and/or thick-walled PS shells with good sphericity and high uniformity of wall thickness is a big challenge all through our target fabrication mission. To tackle this problem, precise control of the micro-encapsulation process is quite critical. As believed, proper choice of the density matching level among the W1, O and W2 phases is one of the most effective approaches. Based on these conclusions, both density matching between the W1 and the O, and that between the W1/O compound droplets and the W2 were intensively studied by Liu *et al.*[33]. They demonstrated that the centering of W1/O compound droplets, the location and movement of W1/O compound droplets in the W2 phase are significantly affected by the density matching level, which leads to variation in wall thickness. However, sphericity of the PS shells is much less sensitive to the
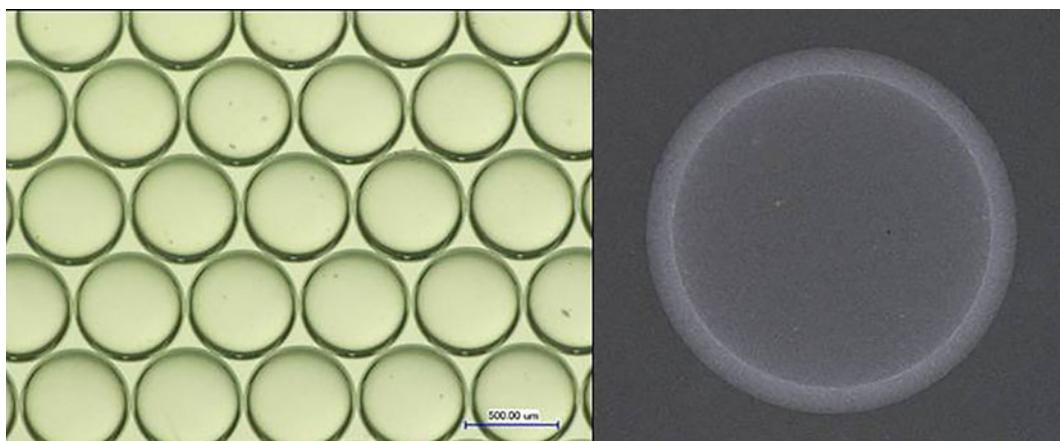
**Figure 7.** Microphotograph of batch PS shells and computed tomography image of individual PS shell.

density matching level. Eventually, as displayed in Figure 7, via further optimization of the density matching level, they have effectively improved the batch uniformity of the wall thickness for the PS shells.

*HDC shell*

Compared to conventional coatings adopted as ICF ablators like GDP and beryllium, HDC coating (including diamond & diamond-like coatings) has several outstanding advantages. Specifically, its high atomic density ensures efficient energy absorption and a high ablation rate as well as effective Rayleigh–Taylor instabilities suppressing; the ultra-high yield strength of HDC enables room temperature handling of fuel filled targets with a pressure around 1000 atm inside; its wide-range optical transparency allows employment of optical techniques to smooth the DT ice layer; and its high thermal conductivity simplifies the cryogenic system[34, 35]. Hence, development of HDC coating is an urgent and meaningful mission for ICF target researchers.

In fact, the superiorities of HDC capsule have been experimentally and theoretically demonstrated by NIC during recent years. We started to explore fabrication of HDC capsule from FY2014, and coupled DC/RF magnetron sputtering technique was employed to deposit HDC films on precise Si mandrels with a diameter of $\sim$2 mm at the beginning. Unfortunately, during the etching process of the mandrel, films on the Si surface tend to fracture and peel off due to the large internal stress, and the density of the film was only $\sim$2.0 g cm$^{-3}$ which was quite smaller than that of diamond ($\sim$3.45 g cm$^{-3}$). During FY2015, a setup designed to fabricate HDC capsules by MP-CVD was built up and put into service. We have investigated dependences of the shell structure, mechanical properties, surface morphology, etc. on parameters like microwave power as well as carbon source. Eventually, uniform HDC coating was successfully



**Figure 8.** Microphotograph of HDC shell.

deposited on Si mandrels. After surface polishing, microfabrication of hole and removal of the silicon mandrel by an etching process, complete hollow HDC shell was acquired eventually as shown in Figure 8. The XRD pattern of such shell displayed in Figure 9 indicates that the shell was mainly composed of diamond phase. Density of the capsule was increased to $\sim$2.7 g cm$^{-3}$, which still needs to be further increased to reach the density of diamond.

## 3. Mechanical machining

All through the mission of target fabrication, various kinds of components like hohlraums, shields, mandrels as well as target knighthead need to be fine machined. After years of upgrade, we have established a versatile machining center equipped with precision diamond lathe, femto-second machining platform, NC linear cutting machine, and so on.
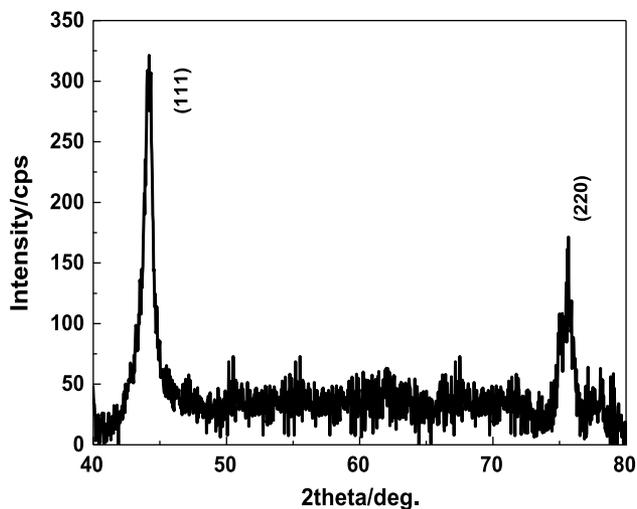
**Figure 9.** XRD pattern of HDC shell.

To meet the ever-changing requirements from ICF scientists, our machining center is undergoing a nonstop upgrade process and fresh machining equipments are brought into service if needed.

With the above machining system at RCLF, we have fulfilled a large amount of experiments and machining missions in time. Li *et al.*[36] used single point precision diamond lathe to machine gold cone target required by fast ignition experiments and drilled micro hole on GDP target shells. At present, both the size precision and thickness uniformity of the gold cone have been noticeably improved to an error of less than 2 µm. They can also drill delicate micro holes on GDP shells with 800 µm in diameter and 20 µm of wall thickness, error of the roundness and size of such hole were limited to below 2 µm. For samples with modulated patterns on the surface used in RT instability experiments, Xie *et al.*[37] have acquired a primary sample by single point precision diamond lathe machining at FY2013. For the initial sample, the minimum machinable peak-valley (PV) value was 1 µm, the maximum breadth ratio was 1, and errors for the breadth and wavelength were ∼0.25 and ∼2 µm, respectively. Figure 10 shows the cutter locus generated by software and the surface morphology measured by atomic force microscopy (AFM) of the corresponding machined modulating surface. By FY2016, adopted confocal optical spectrum displacement measurement theory, they upgraded the diamond lathe with an online measurement and compensation technique. This technique is based on locus error compensation model of modulating curve using a method of least squares. Thanks to this updated technique, silhouette error of the modulating curve was remarkably decreased by an extent of 44.2%. Specifically, the PV value was decreased from ∼1.0 to ∼0.56 µm. Zhang *et al.*[38] utilized precision milling method to fabricate aluminum sleeves; they managed to decrease the burr size at the

detection window to less than 10 µm. The surface roughness of the sleeves was less than 0.1 µm, axiality error was less than 2 µm, size and cylindricity error were limited to smaller than 4 µm. In FY2016, through vac-sorb of GDP shells without contamination and damage, and further assisted by special designed clamp apparatus and diamond cutters, we succeeded to cut square and V-type grooves with excellent precision on the surface of GDP shells.

## 4. Target characterizations

All the target components need to be thoroughly characterized to check their feature deviations from the theoretical blueprint. Only those meeting the error permission could be supplied to the experimental sites. Due to a large amount of diversified target components and their exceptional features, various measurement techniques are necessary and explored by us continually.

In order to acquire a comprehensive characterization of the surface quality of various capsules, Zhao *et al.*[39, 40] have built up a surface mapping technique which is an integration of AFM and fine air bearing rotor. Assisted by the air bearing rotor, locuses along several orthogonal great circles are recorded by the AFM probe working under contact mode. Combinations of these locuses are manipulated by discrete fourier transform into a so-called mode-power spectrum which just contains roughness information of the capsule surface.

Surface step profiler and conventional white-light interferometer (WLI) are usually employed to measure the thickness of films. However, the surface step profiler always tends to cause scratch damages on the film surface, while error of the measured results from WLI is not acceptable sometimes. To improve the accuracy of the thickness measurement, Ma *et al.*[41, 42] proposed a new method based on double confocal sensors. For thickness measurement of freestanding films, two sets of double confocal contactless light sensors are employed to locate front and back surfaces of the films, and the accurate thickness value is derived from calculations of the two detected surface positions. Assisted by an accurate moving motor, the thickness distribution can be further obtained through scanning by the sensors. In FY2016, they proposed another new effective approach to evaluate the thickness distributions of thick freestanding metallic films, which is a significant progress in thickness measurement. With this method, based on opposing white-light interferometry, we can accurately measure the thickness distribution of metallic films not thicker than 500 µm with uncertainty of less than 0.1 µm. Compared to the double surface confocal approach, this method has higher lateral definition and wider applications. Figure 11 shows the thickness distribution obtained by this technique of a sample with complicated profile.
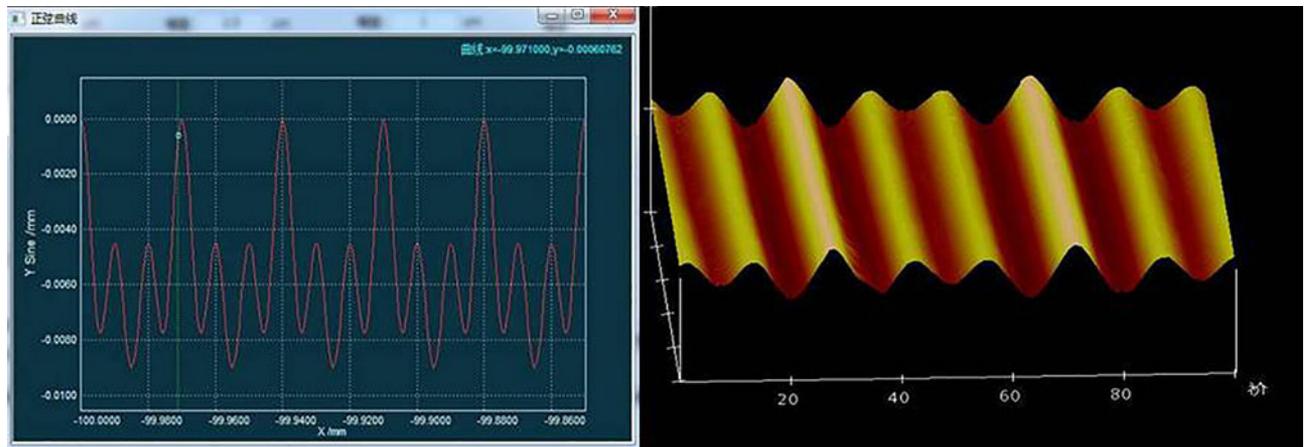
**Figure 10.** Designed locus for the diamond cutter and AFM image of the modulating sample surface.

Based on vertical scanning WLI, other advances in characterizations of target components at RCLF are achieved, which is the realization of nondestructive determination of fuel gas pressure inside the GDP target capsules before they are shot by FY2014. This technique was further improved to be able to detect pressure inside glass capsules by FY2015. Moreover, we have realized the design and setup of a quantitative x-ray photograph system as well as an auxiliary film processing machine, with which we are able to measure the doping amount within the fabricated target components.

## 5. Target assemblies

After the initial fabrication and characterization of different target components, all the components are required to be assembled together according to theoretical design. Since this process involves parts of varied shapes, dimensions and materials, it is also a tough task to manage accurately which is the ultimate decisive factor for the comprehensive quality of the assembled targets.

During the early time of target assembly, most of the target components were assembled manually. As a result, the efficiency was very low, and the assembly accuracy as well as reproducibility was quite limited. Hence, we have dedicated to explore automatic or semi-automatic assembly apparatus and techniques from the beginning. Wu *et al.*[43] have designed a semi-automatic assembly system aimed at the integration of implosive targets. The system is equipped with 21 motor-driven axis and more than three manipulators. At the center of its topological operating space, there are micromanipulators with multi-degrees of freedoms, online monitors, and micro fixtures for target components. With this system, we can realize automatic transfer, online positional inspection and three-dimensional positional adjustments of the target components. The operation space is 40 mm × 40 mm × 50 mm, definition of positioning along XYZ axis
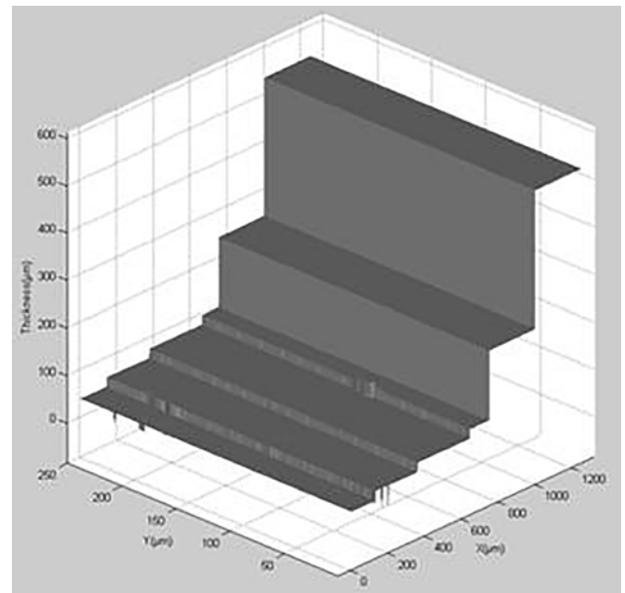


**Figure 11.** Thickness distribution of a complex shaped sample.

is ∼1 μm with repeatable accuracy ⩽2 μm and definition of rotary positioning is ∼0.002°, with repeatable accuracy ⩽0.005°. By FY2015, as exhibited in Figure 12, we built up another semi-automatic assembly system designed for assembly of wire-supported micro-targets.

## 6. Difficulties

Objectively, though we have made lots of achievements on target fabrication in China, we still fail to keep up with the target quality fabricated by NIC, and there is evident distance from our capability to the ever-upgrading requirements from ICF experiments. On September 30, 2010, NIC ended up with failure; it means China on its own will face more
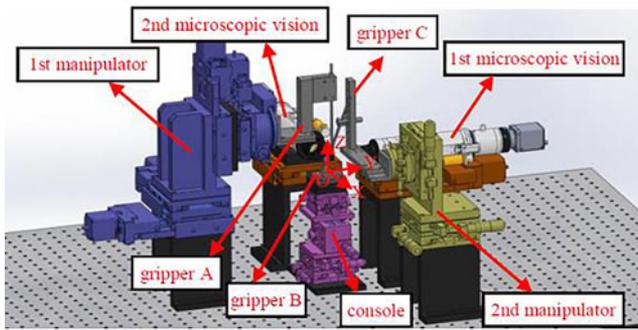
**Figure 12.** Configuration of the semi-automatic assembly system.

challenges and uncertainties with respect to ICF experiments and target fabrication. In order to solve these challenges, we should make full use of the resources available to us, and evaluate possible difficulties in the ICF experiments ahead of schedule through extensive theoretical simulations and experiments independently. Thus, enhanced capability to fabricate target components timely and precisely will be an urgent challenge for target developers at RCLF.

## 7. Conclusions

In summary, fabrication of target components used in ICF experiments is a challenging project involving various scientific topics, materials preparation and manufacture process. Along with the development of ICF experiments, more effective and applicable theories and techniques need to be explored to deal with much more challenges and difficulties ahead. Guided by requirements from ICF experiments and the objective to realize the ultimate utilization of nuclear fusion energy, RCLF will try its best to fabricate target quality components to fulfill its mission within China's ICF campaign.

## Acknowledgements

## References

1.  E. I. Moses, T. D. la Rubia, E. Storm, J. F. Latkowski, J. C. Farmer, R. P. Abbott, K. J. Kramer, P. F. Peterson, H. F. Shaw, and R. F. Lehman, II, Fusion Sci. Technol. **56**, 547 (2009).
2.  Z. Jie, Physics **28**, 142 (1999).
3.  J. Zhang and T. Chang, *Fundaments of the Target Physics for Laser Fusion* (National Defence Industry Press, 2004).
4.  S. W. Haan, M. C. Herrmann, P. A. Amendt, D. A. Callahan, T. R. Dittrich, M. J. Edwards, O. S. Jones, M. M. Marinak, D. H. Munro, S. M. Pollaine, J. D. Salmonson, B. K. Spears, and L. J. Suter, Fusion Sci. Technol. **49**, 553 (2006).
5.  B. A. Hammel and the National Ignition Campaign Team Plasma Phys. Control. Fusion **48**, 497 (2006).
6.  S. W. Haan, D. A. Callahan, M. J. Edwards, B. A. Hammel, D. D. Ho, O. S. Jones, J. D. Lindl, B. J. MacGowan, M. M. Marinak, D. H. Munro, S. M. Pollaine, J. D. Salmonson, B. K. Spears, and L. J. Suter, Fusion Sci. Technol. **55**, 227 (2009).
7.  L. Zhang and K. Du, High Power Laser Part. Beams **25**, 3091 (2013).
8.  Y. Tang, Trends Nucl. Phys. **12**, 50 (1995).
9.  X. Liu, W. Wu, Z. He, B. Zhang, H. Wang, and C. Cai, High Power Laser Part. Beams **21**, 350 (2009).
10. Z. Yang, Z. He, Z. Song, T. Lu, B. Zhang, and Y. Tang, High Power Laser Part. Beams **22**, 1044 (2010).
11. Z. He, Z. Yang, J. Yan, and L. Zhang, At. Energy Sci. Technol. **44**, 989 (2010).
12. J. Yan, Z. He, and Z. Yang, Acta Phys. Sin. **60**, 036501 (2011).
13. B. Zhang, Z. He, W. Wu, X. Liu, and X. Yang, Acta Phys. Sin. **58**, 6436 (2009).
14. B. Zhang, Z. He, W. Wu, X. Yang, and X. Liu, At. Energy Sci. Techol. **43**, 776 (2009).
15. Y. Zhang, Z. He, J. Yan, P. Li, and Y. Tang, Acta Phys. Sin. **60**, 066803 (2011).
16. Y. Zhang, Z. He, P. Li, and J. Yan, Acta Phys. Sin. **60**, 126501 (2011).
17. L. Qiu, Y. Fu, Y. Tang, Y. Wei, Y. Zheng, T. Shi, and S. Yao, Sci. China **45**, 371 (2002).
18. L. Qiu, Y. Fu, X. Wang, S. Wei, and T. Shi, High Power Laser Part. Beams **11**, 465 (1999).
19. X. Qi, S. Wei, Z. Zhang, B. Li, S. Chen, and T. Shi, At. Energy Sci. Technol. **44**, 1371 (2010).
20. X. Qi, Z. Zhang, B. Li, S. Chen, and T. Shi, J. Process Eng. **10**, 109 (2010).
21. X. Qi, C. Gao, Z. Zhang, B. Li, and S. Wei, High Power Laser Part. Beams **24**, 2607 (2012).
22. X. Qi, B. Li, S. Chen, Z. Zhang, and T. Shi, At. Energy Sci. Technol. **44**, 1065 (2010).
23. X. Qi, S. Wei, Z. Zhang, S. Chen, and B. Li, High Power Laser Part. Beams **22**, 2303 (2010).
24. X. Qi, S. Wei, Z. Zhang, B. Li, and S. Chen, High Power Laser Part. Beams **22**, 1543 (2010).
25. S. A. Letts, E. M. Fearon, S. R. Buckley, M. D. Saculla, L. M. Allison, and R. Cook, Fusion Technol. **28**, 1797 (1995).
26. M. L. Hoppe, Fusion Technol. **38**, 42 (2000).
27. M. L. Hoppe, Fusion Sci. Technol. **41**, 234 (2002).
28. W. Xu, T. Wang, Z. He, and Z. Wu, High Power Laser Part. Beams **27**, 062008 (2015).
29. W. Xu, T. Wang, Z. Wu, and Z. He, High Power Laser Part. Beams **27**, 122004 (2015).
30. B. Li, S. Chen, and Z. Zhang, High Power Laser Part. Beams **16**, 1005 (2004).
31. Y. Liu, L. Su, M. Liu, Z. Zhang, B. Li, and S. Chen, High Power Laser Part. Beams **24**, 2677 (2012).
32. S. Chen, B. Li, and Y. Liu, At. Energy Sci. Technol. **16**, 1005 (2009).
33. M. Liu, S. Chen, X. B. Qi, B. Li, R. Shi, Y. Liu, Y. Chen, and Z. Zhang, Chem. Eng. J. **241**, 466 (2014).
34. J. Biener, P. B. Mirkarimi, J. W. Tringe, S. L. Baker, Y. Wang, S. O. Kucheyev, N. E. Teslich, K. J. J. Wu, A. V. Hamza, C. Wild, E. Woerner, P. Koidl, K. Bruehne, and H. J. Fecht, Fusion Sci. Technol. **49**, 737 (2006).
35. J. Biener, D. D. Ho, C. Wild, E. Woerner, M. M. Biener, B. S. El-dasher, D. G. Hicks, J. H. Eggert, P. M. Celliers, G. W. Collins, N. E. Teslich, Jr., B. J. Kozioziemski, S. W. Haan, and A. V. Hamza, Nucl. Fusion **49**, 112001 (2009).

36. G. Li, Y. Huang, W. Tong, and K. Du, Proc. SPIE **8416**, 841628 (2012).
37. J. Xie, Y. Huang, T. Sun, J. Guo, G. Yuan, and W. Tong, At. Energy Sci. Technol. **43**, 279 (2009).
38. H. Zhang, Y. Huang, G. Yuan, Y. Tao, and F. Liu, Manuf. Technol. Mach. Tool **7**, 134 (2012).
39. X. Zhao, D. Gao, X. Ma, J. Meng, Y. Tang, L. Zhang, and T. Sun, At. Energy Sci. Technol. **46**, 1014 (2012).
40. X. Zhao, T. Sun, D. Gao, Y. Tang, and S. Dong, High Power Laser Part. Beams **17**, 1847 (2005).
41. X. Ma, D. Gao, M. Yang, X. Zhao, C. Ye, and Y. Tang, Opt. Precis. Eng. **19**, 17 (2011).
42. M. Yang, P. Xing, D. Gao, X. Ma, and C. Li, At. Energy Sci. Technol. **44**, 576 (2010).
43. W. R. Wu, D. H. Yu, and L. Zhang, Adv. Mater. Res. **605**, 1431 (2013).